Factors Influencing the Irreversible Oxygen Loss and Reversible Capacity in Layered $Li[Li_{1/3}Mn_{2/3}]O_2-Li[M]O_2$ ($M = Mn_{0.5-y}Ni_{0.5-y}Co_{2y}$ and $Ni_{1-y}Co_y$) Solid Solutions

T. A. Arunkumar, Y. Wu, and A. Manthiram*

Materials Science and Engineering Program, The University of Texas at Austin, Austin, Texas 78712

Received February 7, 2007. Revised Manuscript Received April 16, 2007

The electrochemical charge−discharge properties of the layered $(1 - z)Li[Li_{1/3}Mn_{2/3}]O_2 \cdot (z)Li[Mn_{0.5-y}Ni_{0.5-y}Co_{2y}]O_2$ ($y = 1/12$, 1/6, and 1/3 and $0.25 \le z \le 0.75$) and $(1 - z)Li[Li_{1/3}Mn_{2/3}]O_2 \cdot (z)Li[Ni_{1-y}Co_y]O_2$ ($0 \le y \le 1$ and $0.2 \le z \le 0.7$) solid solution series have been investigated with an aim to identify the factors that control the amount of oxygen loss from the lattice during the first charge and the reversible capacity values. The first charge profiles exhibit an initial sloping region A followed by a plateau region B around 4.5 V. The sloping region A is found to be determined by the initial average oxidation state of the transition metal ions and their oxidation to Ni^{4+} and $Co^{3.6+}$ with Mn remaining as Mn^{4+}. The plateau region B, which corresponds to an irreversible loss of oxygen from the lattice, is found to be determined by the amount of lithium η in the transition metal layer of the solid solution $Li[Li_\eta M_{1-\eta}]O_2$. However, high Mn^{4+} content causes a decrease in oxygen mobility and loss. Moreover, the tendency of Ni^{3+} to get reduced to Ni^{2+} and the consequent volatilization of lithium during synthesis alter the lithium content in the transition metal layer and thereby influence the degree of oxygen loss and reversible capacity values.

Introduction

Lithium ion batteries have revolutionized the portable electronics market since their commercialization first by Sony Corporation in 1990. They are also being intensively pursued for electric and hybrid electric vehicle applications. Lithium ion cells for portable electronic devices such as cell phones and laptop computers are currently made largely with the layered $LiCoO_2$ cathode. However, only 50% of the theoretical capacity of $LiCoO_2$ can be utilized in practical cells because of the chemical and structural instabilities at deep charge with $(1 - x) < 0.5$ in $Li_{1-x}CoO_2$[1,2] as well as safety concerns. These drawbacks together with the high cost and toxicity of Co have created enormous interest in alternative cathodes. In this regard, solid solutions between layered $Li[Li_{1/3}Mn_{2/3}]O_2$ (commonly designated as Li_2MnO_3) and $LiMO_2$ ($M = Mn_{0.5}Ni_{0.5}$, Co, Ni, and Cr) have become appealing as they exhibit a high reversible capacity of around 250 mA·h/g with a lower cost and better safety compared to the currently used $LiCoO_2$ cathode.[3−13] Although Li_2MnO_3 is electrochemically inactive as it is difficult to oxidize beyond Mn^{4+}, its solid solutions with other $LiMO_2$ oxides exhibit good electrochemical activity.

However, the $Li[Li_{1/3}Mn_{2/3}]O_2-LiMO_2$ solid solutions exhibit two distinct regions during the first charge.[3−13] While the initial sloping region corresponds to the oxidation of the transition metal ions to M^{4+}, the following plateau region around 4.5 V corresponds to an irreversible loss of oxygen from the lattice as has been confirmed by in situ X-ray diffraction[5] and differential electrochemical mass spectrometry studies.[12] The lithium extraction accompanying the oxygen loss facilitates the lowering of the oxidation states of the transition metal ions at the end of the first discharge and thereby a high reversible capacity in the subsequent charge−discharge cycles.

However, the amount of oxygen loss from the lattice and the reversible capacity values differ significantly depending upon the composition of the $Li[Li_{1/3}Mn_{2/3}]O_2-LiMO_2$ solid solutions. With an aim to understand the factors that control the degree of oxygen loss and the subsequent capacity values, we present here a systematic investigation of the charge−discharge behavior of a number of layered oxide solid solutions belonging to the series $(1 - z)Li[Li_{1/3}Mn_{2/3}]O_2 \cdot (z)Li[M]O_2$ ($M = Mn_{0.5-y}Ni_{0.5-y}Co_{2y}$ and $Ni_{1-y}Co_y$).

* To whom correspondence should be addressed. Phone: 512-471-1791. Fax: 512-471-7681. E-mail: rmanth@mail.utexas.edu.

(1) Chebiam, R. V.; Prado, F.; Manthiram, A. *Chem. Mater.* **2001**, *13*, 2951.
(2) Venkatraman, S.; Shin, Y.; Manthiram, A. *Electrochem. Solid-State Lett.* **2003**, *6*, A9.
(3) Numata, K.; Sakaki, C.; Yamanaka, S. *Solid State Ionics* **1999**, *117*, 257.
(4) Lu, Z.; Beaulieu, L. Y.; Donaberger, R. A.; Thomas, C. L.; Dahn, J. R. *J. Electrochem. Soc.* **2002**, *149*, A778.
(5) Lu, Z.; Dahn, J. R. *J. Electrochem. Soc.* **2002**, *149*, A815.
(6) Lu, Z.; Dahn, J. R. *J. Electrochem. Soc.* **2002**, *149*, A1454.
(7) Zhang, L.; Noguchi, H.; Yoshio, M. *J. Power Sources* **2002**, *110*, 57.
(8) Kang, S. H.; Sun, Y. K.; Amine, K. *Electrochem. Solid-State Lett.* **2003**, *6*, A183.
(9) Park, Y. J.; Hong, Y. S.; Wu, X.; Ryu, K. S.; Chang, S. H. *J. Power Sources* **2004**, *129*, 288.
(10) Park, Y. J.; Wu, X.; Hong, Y. S.; Ryu, K. S.; Chang, S. H. *Solid State Ionics* **2004**, *175*, 305.
(11) Whitfield, P. S.; Niketic, S.; Davidson, I. J. *J. Power Sources* **2005**, *146*, 617.
(12) Armstrong, A. R.; Holzapfel, M.; Novak, P.; Johnson, C. S.; Kang, S.; Thackeray, M. M.; Bruce, P. G. *J. Am. Chem. Soc.* **2006**, *128*, 8694.
(13) Wu, Y.; Manthiram, A. *Electrochem. Solid-State Lett.* **2006**, *9*, A221.

10.1021/cm070389q CCC: $37.00
Published on Web 05/22/2007

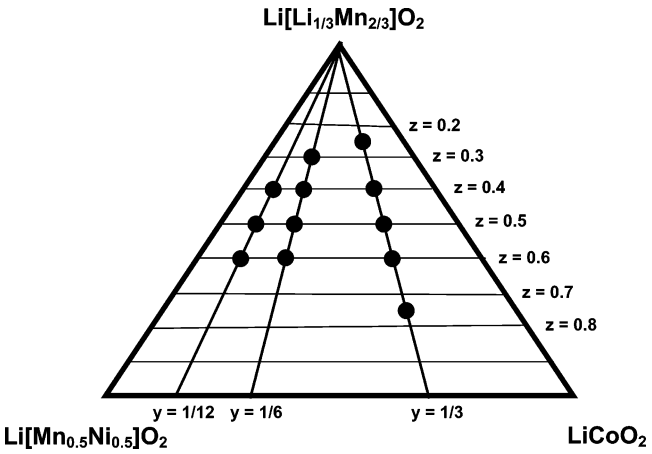

Figure 1. Phase diagram of the $Li[Li_{1/3}Mn_{2/3}]O_2-Li[Mn_{0.5}Ni_{0.5}]O_2-LiCoO_2$ system. The compositions studied in the $(1-z)Li[Li_{1/3}Mn_{2/3}]O_2\cdot(z)Li[Mn_{0.5-y}Ni_{0.5-y}Co_{2y}]O_2$ ($y = 1/3$, 1/6, and 1/12 and $0.25 \le z \le 0.75$) system are indicated by closed circles.

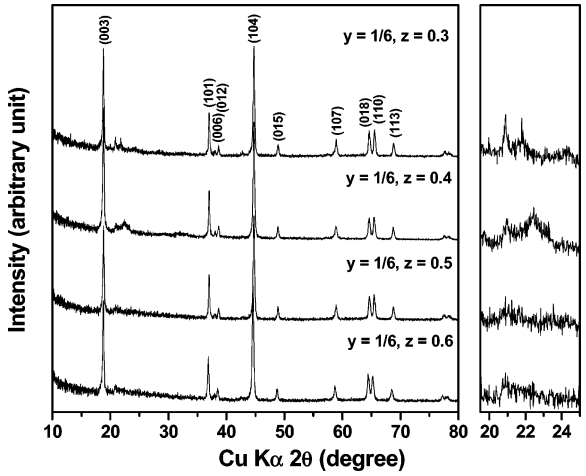

Figure 2. XRD patterns of the $(1-z)Li[Li_{1/3}Mn_{2/3}]O_2\cdot(z)Li[Mn_{0.5-y}Ni_{0.5-y}Co_{2y}]O_2$ ($y = 1/6$ and $0.3 \le z \le 0.6$) samples. The expanded region on the right shows the superstructure reflections arising from an ordering among Li^+, Mn^{4+}, and Ni^{2+}.

Experimental Section

All the samples presented in this study were synthesized by a coprecipitation method in which the hydroxide precursors of the transition metal ions were first precipitated from a solution containing required quantities of manganese, nickel, and cobalt acetates by adding KOH, followed by firing the oven-dried hydroxide precursors with a required amount of $LiOH\cdot H_2O$ at 900 °C for 12 h in air and quenching into liquid nitrogen. All the products were characterized by X-ray diffraction with Cu Kα radiation. Lithium contents in the synthesized samples were determined by atomic absorption spectroscopy (AAS). The average oxidation state of the transition metal ions present in the samples was determined by treating the samples with a known excess of sodium oxalate and titrating the unreacted sodium oxalate with potassium permanganate.

Electrochemical performances were evaluated with CR2032 coin cells at 12.5 mA/g (~*C*/20 rate) between 4.8 and 2.0 V. The coin cells were fabricated with the layered oxide cathodes, metallic lithium anode, 1 M $LiPF_6$ in 1:1 diethyl carbonate/ethylene carbonate electrolyte and a Celgard polypropylene separator. The cathodes were prepared by mixing 75 wt % active material with 20 wt % conductive carbon and 5 wt % polytetrafluoroethylene (PTFE) binder, rolling the mixture into thin sheets, and cutting into circular electrodes of 0.64 cm^2 area. The electrodes typically had an active material content of ~7 mg.

Results and Discussion

$Li[Li_{1/3}Mn_{2/3}]O_2-Li[Mn_{0.5-y}Ni_{0.5-y}Co_{2y}]O_2$ Solid Solution. The compositions studied in the $(1-z)Li[Li_{1/3}Mn_{2/3}]O_2\cdot(z)Li[Mn_{0.5-y}Ni_{0.5-y}Co_{2y}]O_2$ ($y = 1/12$, 1/6, and 1/3 and $0.25 \le z \le 0.75$) solid solution series are indicated by closed circles in Figure 1. X-ray diffraction data indicated all the samples to be single phase materials belonging to the α-$NaFeO_2$ layered structure (O3 structure). However, in addition to the reflections corresponding to the O3 layered structure, weak superstructure reflections were observed around $2\theta = 20-25°$ for samples with high $Li[Li_{1/3}Mn_{2/3}]O_2$ content, which are known to correspond to the ordering of the Li^+, Ni^{2+}, and Mn^{4+} ions in the transition metal layer of the layered lattice.[4,6] For example, the X-ray diffraction patterns of the $y = 1/6$ series of samples are given in Figure 2 for various values of *z*. The superstructure reflections become less pronounced as the value of *z* increases as evident from the expanded region shown on the right in Figure 2. Chemical analysis indicated the Li content in the synthesized samples to be similar to that in the nominal compositions for all these series of samples. The transition metal ions are known to exist as Mn^{4+}, Ni^{2+}, and Co^{3+} in these materials. The observed compositions based on the experimentally determined lithium content and average oxidation state of the transition metal ions (M^{n+}) are given in Table 1.

Figure 3 compares the first charge−discharge profiles of the $(1-z)Li[Li_{1/3}Mn_{2/3}]O_2\cdot(z)Li[Mn_{0.5-y}Ni_{0.5-y}Co_{2y}]O_2$ ($0.25 \le z \le 0.75$) solid solution samples for $y = 1/3$ at 2.0−4.8 V. The first charge and discharge capacity values are given in Table 1. The samples in Figure 3 exhibit two regions (A and B) in the first charge profiles that are separated by a dashed vertical line. While the initial sloping region A below about 4.5 V corresponds to the oxidation of the transition metal ions, the plateau region B around 4.5 V corresponds to an oxidation of O^{2-} ions and an irreversible loss of oxygen from the lattice as pointed out earlier in the introduction.[3−13] Except at a high $Li[Li_{1/3}Mn_{2/3}]O_2$ content or low *z* value (0.25), the first total charge capacity (regions A + B) and the discharge capacity decrease with increasing *z* or decreasing lithium content η in the transition metal layer in $Li[Li_\eta M_{1-\eta}]O_2$ for the $y = 1/3$ series of samples. Also, while the first charge capacity in the initial sloping region A increases, that in the plateau region B decreases with decreasing lithium content η in the transition metal layer as seen in Table 1 and Figure 4a for the $y = 1/3$ series of samples. The former is due to an increasing amount of Co^{3+} and Ni^{2+} ions (or a decrease in the average oxidation state of the transition metal ions) in the samples that could get oxidized during first charge. Table 1 gives the theoretical value of the first charge capacity calculated on the basis of the oxidation of the transition metal ions to Mn^{4+}, Ni^{4+}, and $Co^{3.6+}$. The calculated first charge capacity value agrees closely with the observed value in the sloping region A, suggesting that it may be difficult to oxidize Co beyond 3.6+ without oxidizing the oxide ions. This could be due to a significant overlap of the $Co^{3+/4+}$:3d band with the top of

Table 1. Observed Chemical Compositions and Electrochemical Data of the Solid Solution Cathodes

				first charge capacity[a] (mA·h/g)						
y	*z*	observed composition	M^{n+}	region A	region B	total (A + B)	calculated capacity in region A[b] (mA·h/g)	first discharge capacity (mA·h/g)	IRC[c] (mA·h/g)	calculated oxygen loss[d]
				$(1-z)Li[Li_{1/3}Mn_{2/3}]O_2\cdot(z)Li[Mn_{0.5-y}Ni_{0.5-y}Co_{2y}]O_2$						
1/3	0.25	$Li[Li_{0.25}Mn_{0.54}Ni_{0.04}Co_{0.17}]O_2$	3.67	70	256	326	59	210	116	0.5
	0.4	$Li[Li_{0.2}Mn_{0.47}Ni_{0.06}Co_{0.27}]O_2$	3.5	95	239	334	92	254	80	0.4
	0.5	$Li[Li_{0.16}Mn_{0.43}Ni_{0.08}Co_{0.33}]O_2$	3.38	120	205	325	118	252	73	0.32
	0.6	$Li[Li_{0.13}Mn_{0.37}Ni_{0.1}Co_{0.4}]O_2$	3.29	135	185	320	134	239	81	0.26
	0.75	$Li[Li_{0.08}Mn_{0.29}Ni_{0.13}Co_{0.5}]O_2$	3.17	165	126	291	162	215	76	0.16
1/6	0.3	$Li[Li_{0.22}Mn_{0.58}Ni_{0.1}Co_{0.1}]O_2$	3.56	85	214	299	95	218	81	0.44
	0.4	$Li[Li_{0.2}Mn_{0.54}Ni_{0.13}Co_{0.13}]O_2$	3.5	110	218	328	110	253	75	0.40
	0.5	$Li[Li_{0.16}Mn_{0.51}Ni_{0.17}Co_{0.17}]O_2$	3.38	135	169	304	140	231	73	0.32
	0.6	$Li[Li_{0.13}Mn_{0.47}Ni_{0.2}Co_{0.2}]O_2$	3.29	150	140	290	159	227	63	0.26
1/12	0.4	$Li[Li_{0.2}Mn_{0.56}Ni_{0.17}Co_{0.07}]O_2$	3.5	115	213	328	117	254	74	0.40
	0.5	$Li[Li_{0.16}Mn_{0.55}Ni_{0.21}Co_{0.08}]O_2$	3.38	145	149	294	150	210	84	0.32
	0.6	$Li[Li_{0.11}Mn_{0.53}Ni_{0.26}Co_{0.1}]O_2$	3.25	160	104	264	187	191	73	0.22
				$(1-z)Li[Li_{1/3}Mn_{2/3}]O_2\cdot(z)Li[Ni_{1-y}Co_y]O_2$						
0.5	0.2	$Li[Li_{0.27}Mn_{0.53}Ni_{0.1}Co_{0.1}]O_2$	3.74	65	188	253	53	168	85	0.54
	0.3	$Li[Li_{0.21}Mn_{0.48}Ni_{0.155}Co_{0.155}]O_2$	3.53	110	200	310	97	205	105	0.42
	0.4	$Li[Li_{0.16}Mn_{0.42}Ni_{0.21}Co_{0.21}]O_2$	3.38	130	189	319	133	200	119	0.32
	0.5	$Li[Li_{0.12}Mn_{0.36}Ni_{0.26}Co_{0.26}]O_2$	3.27	150	155	305	159	205	100	0.24
	0.6	$Li[Li_{0.08}Mn_{0.28}Ni_{0.32}Co_{0.32}]O_2$	3.17	180	113	293	183	208	85	0.16
	0.7	$Li[Li_{0.05}Mn_{0.21}Ni_{0.37}Co_{0.37}]O_2$	3.11	215	57	272	200	220	52	0.10
0	0.5	$Li[Li_{0.08}Mn_{0.37}Ni_{0.55}]O_2$	3.17	234	0[e]	234	220	194	40	0.16
0.25		$Li[Li_{0.10}Mn_{0.36}Ni_{0.41}Co_{0.13}]O_2$	3.22	185	92	277	190	208	69	0.20
0.5		$Li[Li_{0.12}Mn_{0.36}Ni_{0.26}Co_{0.26}]O_2$	3.27	150	155	305	159	205	100	0.24
0.75		$Li[Li_{0.14}Mn_{0.34}Ni_{0.13}Co_{0.39}]O_2$	3.33	135	181	316	127	233	83	0.28
1		$Li[Li_{0.17}Mn_{0.33}Co_{0.5}]O_2$	3.41	100	233	333	92	269	64	0.34

[a] Regions A and B correspond to respectively the initial sloping region A and the plateau region B in the charge profile. [b] Calculated assuming the oxidation of Mn, Ni, and Co respectively to Mn^{4+}, Ni^{4+}, and $Co^{3.6+}$. [c] Refers to irreversible capacity loss, which is the difference between the first charge and the first discharge capacity values. [d] Calculated on the basis of the maximum amount of oxygen the sample could lose (see text). [e] The sample does not show a clearly recognizable plateau region.

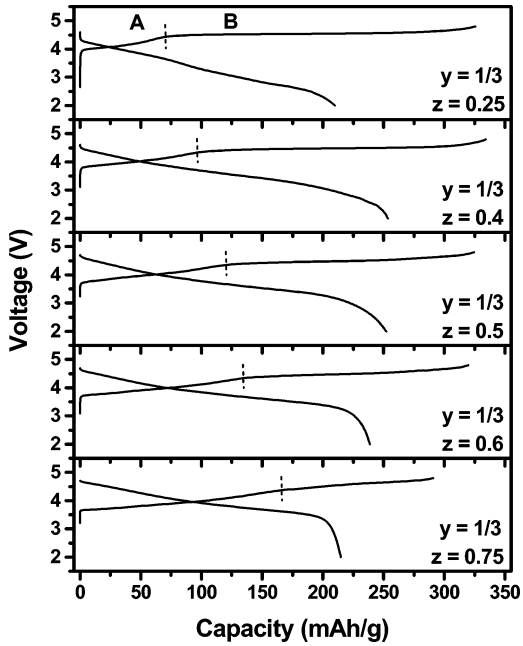

Figure 3. Comparison of the first charge−discharge profiles (recorded at 12.5 mA/g between 2.0 and 4.8 V) of the $(1-z)Li[Li_{1/3}Mn_{2/3}]O_2\cdot(z)Li[Mn_{0.5-y}Ni_{0.5-y}Co_{2y}]O_2$ ($y = 1/3$ and $0.25 \le z \le 0.75$) samples. The dashed vertical lines separate the initial sloping region A from the plateau region B.

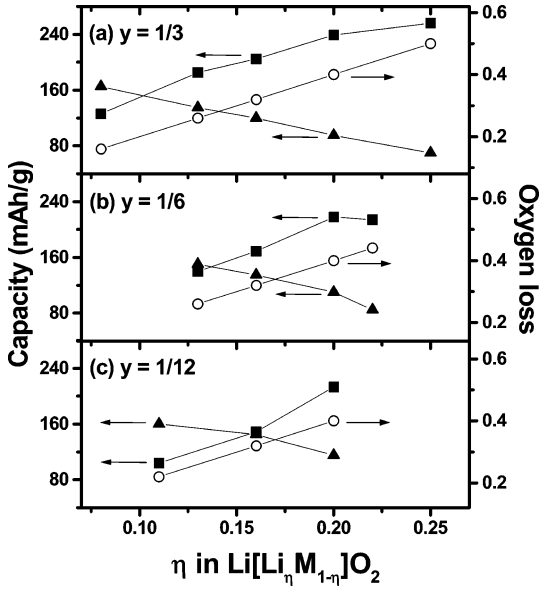

Figure 4. Variations of the first charge capacity in region A (▲) and region B (■) and the calculated oxygen loss (○) with lithium content η in the transition metal layer of the $(1-z)Li[Li_{1/3}Mn_{2/3}]O_2\cdot(z)Li[Mn_{0.5-y}Ni_{0.5-y}Co_{2y}]O_2$ solid solution samples.

the O^{2-}:2p band and a consequent introduction of holes into the O^{2-}:2p band and oxidation of O^{2-} ions for oxidations beyond $Co^{3.6+}$. This is consistent with the limited practical capacity (50%) of $LiCoO_2$ and the chemical instability of $Li_{1-x}CoO_2$ for $(1-x) < 0.5$ as revealed by the chemical characterization of chemically delithiated samples.[1,2] On the other hand, the irreversible capacity loss in the first cycle (difference between the first charge and the discharge capacities) does not show any clear relationship.

The decrease in the first charge capacity values in the plateau region B and the consequent decrease in the discharge capacity values with decreasing lithium content η in the transition metal layer could be understood by considering a mechanism proposed by Armstrong et al.[12] recently for the

system $Li[Li_{0.2}Mn_{0.6}Ni_{0.2}]O_2$, which is a solid solution between $Li[Li_{1/3}Mn_{2/3}]O_2$ and $Li[Mn_{0.5}Ni_{0.5}]O_2$. On the basis of electrochemical mass spectrometry and powder neutron diffraction data, they suggested that the oxygen loss from the surface of the particle is accompanied by a migration of Li^+ ions from the octahedral sites of the transition metal layer into the octahedral sites of the lithium layer. The cation vacancies generated in the transition metal layer by this migration process are then filled by a cooperative diffusion of the transition metal ions from the surface into the bulk of the particle and rearrangement. On the basis of this consideration, the oxygen loss from the lattice will cease when all the cation vacancies in the transition metal layer are filled by the transition metal ions to give $[M]O_2$. Thus, the limiting oxygen content value in the fully charged sample will be twice the transition metal ion content, or the maximum amount of oxygen loss from the lattice will be equal to twice the amount of lithium in the transition metal layer. In essence, the higher the lithium content η in the transition metal layer in $Li[Li_\eta M_{1-\eta}]O_2$, the lower will be the transition metal content $(1 - \eta)$ and the higher will be the oxygen loss from the lattice during the first charge.

On the basis of the above hypothesis, the maximum amount of oxygen loss that could occur for each sample is given as calculated oxygen loss in Table 1. For example, the $Li[Li_{0.2}Mn_{0.47}Ni_{0.06}Co_{0.27}]O_{2-\delta}$ ($y = 1/3$ and $z = 0.4$) sample has to maintain an oxygen content of 1.6 at the end of first charge to keep the ratio between transition metal ions and oxygen as 1:2, amounting to a calculated oxygen loss of 0.4. In other words, the limiting composition for the sample with $y = 1/3$ and $z = 0.4$ at the end of first charge will be $[Mn_{0.47}Ni_{0.06}Co_{0.27}]O_{1.6}$, which on rearrangement (normalizing the oxygen content to 2.0) will give $[Mn_{0.59}Ni_{0.07}Co_{0.34}]O_2$, with all the transition metal ions in the 4+ oxidation state. The decrease in the calculated oxygen loss with increasing z value (or decreasing lithium content in the transition metal layer) leads to a decrease in the plateau region B and a consequent decrease in the discharge capacity with increasing z as seen in Table 1 and Figures 3 and 4a for the $y = 1/3$ series of samples.

Similar to the 1/3 series of samples, the $y = 1/6$ and 1/12 series of samples in the $(1 - z)Li[Li_{1/3}Mn_{2/3}]O_2 \cdot (z)Li[Mn_{0.5-y}Ni_{0.5-y}Co_{2y}]O_2$ ($0.25 \le z \le 0.75$) solid solution series also exhibit an initial sloping region A followed by a plateau region B in the first charge profile. The observed compositions based on the experimentally determined lithium content and oxidation state values as well as the first charge and discharge capacity values are given in Table 1. At a given z value, the $y = 1/6$ and 1/12 series of samples have lower Co content and higher Mn and Ni contents compared to the $y = 1/3$ samples. The first total charge capacity (regions A + B) and the discharge capacity decrease with increasing z or decreasing lithium content η in the transition metal layer for the $y = 1/6$ and 1/12 series of samples also similar to that found for the $y = 1/3$ series of samples except for the $y = 1/6$ and $z = 0.3$ sample with high $Li[Li_{1/3}Mn_{2/3}]O_2$ content. Figure 4b,c shows the variations of the first charge capacity in regions A and B and the calculated oxygen loss with lithium content η in the transition metal layer for the

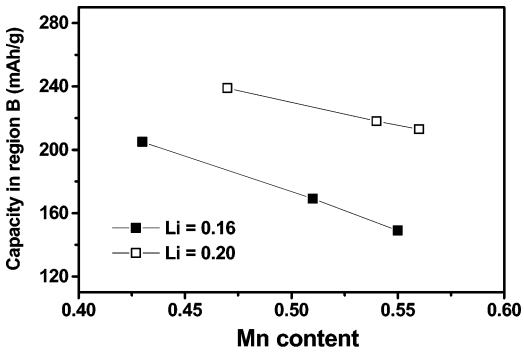

Figure 5. Variations of the first charge capacity in the plateau region B with Mn content in samples having a similar lithium content in the $(1 - z)Li[Li_{1/3}Mn_{2/3}]O_2 \cdot (z)Li[Mn_{0.5-y}Ni_{0.5-y}Co_{2y}]O_2$ solid solution.

$y = 1/6$ and 1/12 series of samples. The initial sloping region A increases, and the plateau region B decreases with increasing z (or decreasing lithium content η in the transition metal layer) similar to the $y = 1/3$ series of samples, respectively, as a result of an increasing amount of Co^{3+} and Ni^{2+} ions (or a decreasing average oxidation state of transition metal ions) that could get oxidized and a decreasing amount of oxygen that could be lost from the lattice during first charge. Thus the data with the $y = 1/6$ and 1/12 series of samples also support the oxygen loss mechanism discussed with the $y = 1/3$ series of samples. Moreover, a close agreement between the observed and the calculated charge capacities in the initial sloping region A support the beginning of oxygen evolution from the lattice for oxidations beyond approximately $Co^{3.6+}$ as in the case of the $y = 1/3$ series of samples. Although the irreversible capacity loss decreases slightly with increasing z in the $y = 1/6$ series, it does not show any clear dependence on z in the $y = 1/12$ series.

Comparing the three series of samples in Table 1 with $y = 1/3$, 1/6, and 1/12 in $(1 - z)Li[Li_{1/3}Mn_{2/3}]O_2 \cdot (z)Li[Mn_{0.5-y}Ni_{0.5-y}Co_{2y}]O_2$, the nature of transition metal ions also has an influence in addition to the lithium content in the transition metal layer in determining the charge and discharge capacity values. For example, with a constant z value of 0.5 or a constant lithium content of 0.16 in the transition metal layer, the plateau region B, total first charge capacity, and first discharge capacity decrease with decreasing Co content $2y$. This is due to an increasing amount of electrochemically inactive Mn^{4+} and the consequent decrease in the oxygen mobility to leave the lattice. For example, Figure 5 illustrates the decrease in the first charge capacity in the plateau region B with increasing Mn content in two series of samples having similar lithium contents of 0.16 and 0.20. This is supported further by the deviations of the $z = 0.25$ sample in the $y = 1/3$ series and the $z = 0.3$ sample in the $y = 1/6$ series with high $Li[Li_{1/3}Mn_{2/3}]O_2$ or Mn^{4+} content from the expected trend in the total charge and discharge capacity values. On the other hand, with a constant z value of 0.5, the initial sloping region A increases with decreasing Co content $2y$ (or increasing Ni^{2+} and Mn^{4+} contents) despite the same average oxidation state of 3.38+ because Ni^{2+} could be fully oxidized to the 4+ state while Co^{3+} could be oxidized only to ~3.6+ before the oxygen evolution from the lattice begins (see the earlier discussion on comparing the observed and

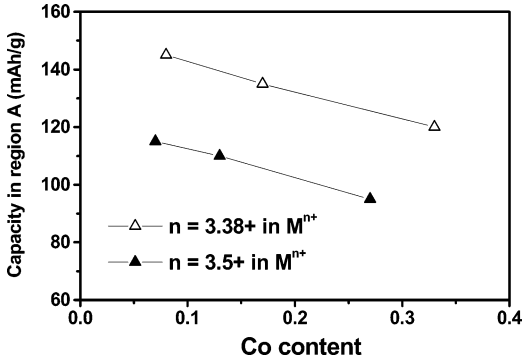

Figure 6. Variations of the first charge capacity in region A with Co content in samples having a similar average oxidation state (M^{n+}) in the $(1-z)$Li[Li$_{1/3}$Mn$_{2/3}$]O$_2$·(z)Li[Mn$_{0.5-y}$Ni$_{0.5-y}$Co$_{2y}$]O$_2$ solid solution.

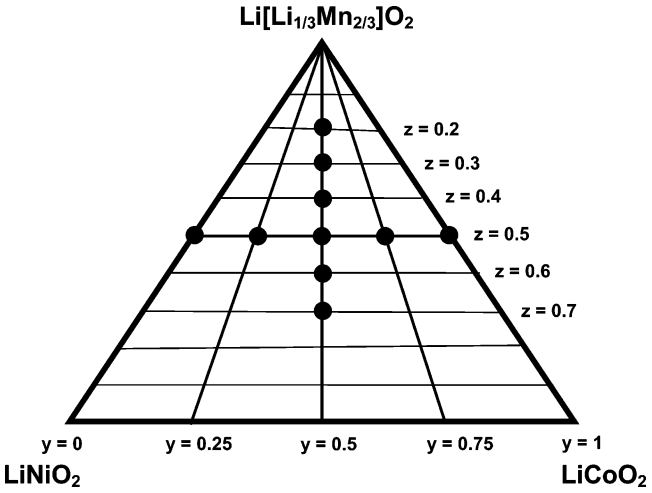

Figure 7. Phase diagram of the Li[Li$_{1/3}$Mn$_{2/3}$]O$_2$−LiNiO$_2$−LiCoO$_2$ system. The compositions studied in the $(1-z)$Li[Li$_{1/3}$Mn$_{2/3}$]O$_2$·(z)Li[Ni$_{1-y}$Co$_y$]O$_2$ ($0 \le y \le 1$ and $0.2 \le z \le 0.7$) system are indicated by closed circles.

calculated charge capacities in region A in Table 1). For example, Figure 6 illustrates the decrease in the first charge capacity in region A with increasing Co content in two series of samples having similar average oxidation states (M^{n+}) of 3.38+ and 3.5+.

Li[Li$_{1/3}$Mn$_{2/3}$]O$_2$−Li[Ni$_{1-y}$Co$_y$]O$_2$ Solid Solution. The compositions studied in the $(1-z)$Li[Li$_{1/3}$Mn$_{2/3}$]O$_2$·(z)Li[Ni$_{1-y}$Co$_y$]O$_2$ ($0 \le y \le 1$ and $0.2 \le z \le 0.7$) solid solution series are indicated by closed circles in Figure 7. X-ray diffraction data indicated the samples to be single phase materials belonging to the O3 type layered structure similar to the previous series of samples, with weak superstructure reflections around $2\theta = 20-25°$ due to the ordering of the Li^+, Ni^{2+}, and Mn^{4+} ions in the transition metal layer of the layered lattice. For example, the X-ray diffraction patterns of the $y = 0.5$ series of samples are given in Figure 8 for various values of z. The superstructure reflections vanish for $z > 0.5$ as seen in the expanded region on the right in Figure 8. Figure 9 shows the variations of the unit cell parameters of the $y = 0.5$ series of samples with z in $(1-z)$Li[Li$_{1/3}$Mn$_{2/3}$]-O$_2$·(z)Li[Ni$_{1-y}$Co$_y$]O$_2$. The a parameter and the unit cell volume increase with the z value while the c parameter and the c/a ratio decrease, illustrating the formation of solid solutions. Similar trends were observed for other solid solution series studied in this work as well.

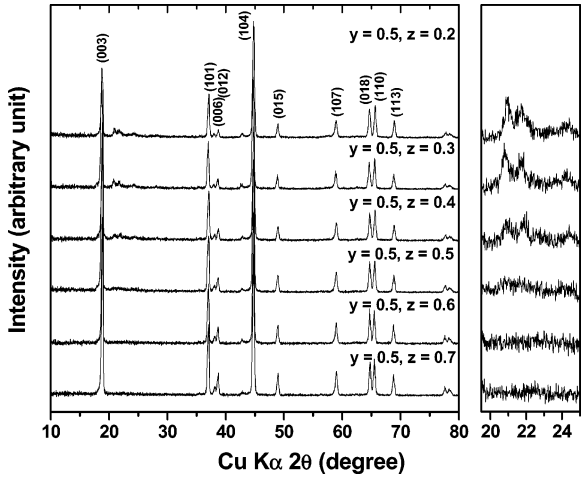

Figure 8. XRD patterns of the $(1-z)$Li[Li$_{1/3}$Mn$_{2/3}$]O$_2$·(z)Li[Ni$_{1-y}$Co$_y$]O$_2$ ($y = 0.5$ and $0.2 \le z \le 0.7$) samples. The expanded region on the right shows the superstructure reflections arising from an ordering among Li^+, Mn^{4+}, and Ni^{2+}.

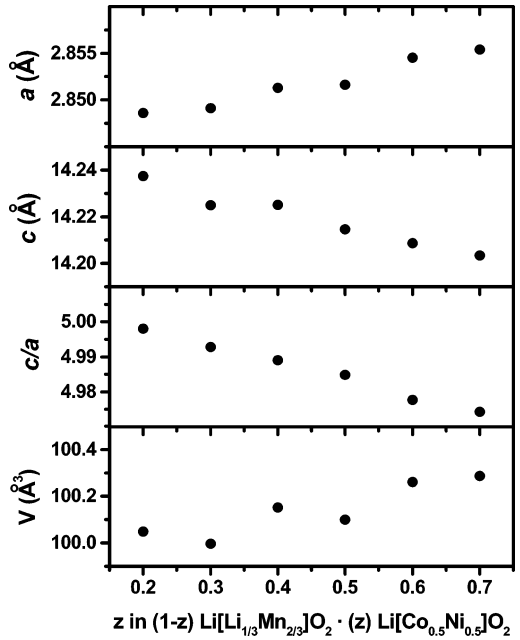

Figure 9. Variations of the unit cell parameters with z for the $y = 0.5$ series of samples in the $(1-z)$Li[Li$_{1/3}$Mn$_{2/3}$]O$_2$·(z)Li[Ni$_{1-y}$Co$_y$]O$_2$ ($0 \le y \le 1$ and $0.2 \le z \le 0.7$) system.

Chemical analysis indicated the lithium content in the synthesized samples to be lower than that in the nominal compositions for these series of samples. The oxidation state analysis by the redox titration indicated the nickel oxidation state to be lower than the expected value of 3+ assuming Li^+, Mn^{4+}, and Co^{3+}. The nickel oxidation state was found to be around 2.52+ to 2.70+ for the $y = 0.5$ and $0.3 \le z \le 0.7$ series of samples and around 2.62+ to 2.54+ for the $0 \le y \le 1$ and $z = 0.5$ series of samples. Thus, the lower lithium content in the samples is due to a reduction of Ni^{3+} to Ni^{2+} and the consequent volatilization of lithium during synthesis at elevated temperatures (900 °C). For a comparison, no such volatilization of lithium was encountered in the previous series of $(1-z)$Li[Li$_{1/3}$Mn$_{2/3}$]O$_2$·(z)Li[Mn$_{0.5-y}$-Ni$_{0.5-y}$Co$_{2y}$]O$_2$ samples as nickel remains as Ni^{2+} in the nominal compositions of this series. The observed compositions based on the experimentally determined lithium content

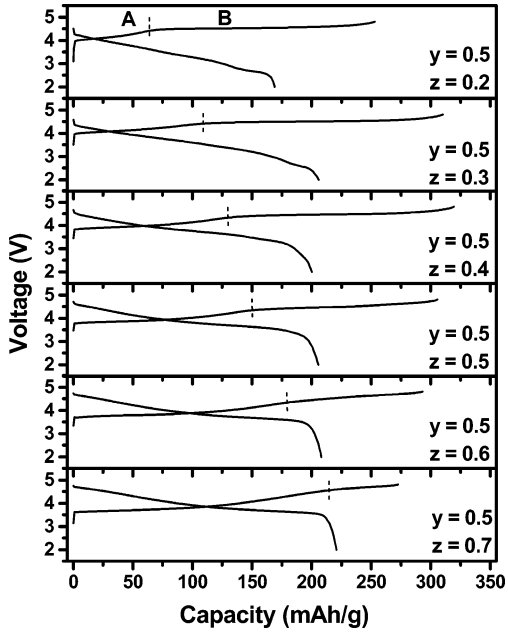

Figure 10. Comparison of the first charge−discharge profiles (recorded at 12.5 mA/g between 2.0 − 4.8 V) of the $(1 - z)Li[Li_{1/3}Mn_{2/3}]O_2 \cdot (z)Li[Ni_{1-y}Co_y]O_2$ ($y = 0.5$ and $0.2 \leq z \leq 0.7$) samples. The dashed vertical lines separate the initial sloping region A from the plateau region B.

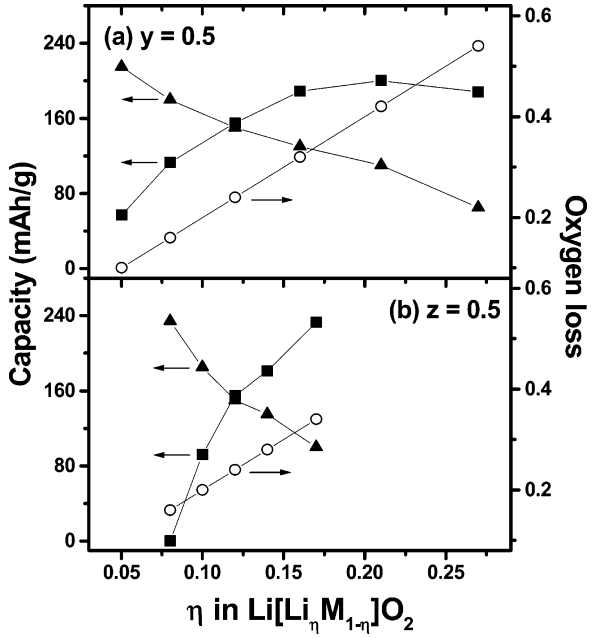

Figure 11. Variations of the first charge capacity in region A (▲) and region B (■) and the calculated oxygen loss (○) with lithium content η in the transition metal layer of the $(1 - z)Li[Li_{1/3}Mn_{2/3}]O_2 \cdot (z)Li[Ni_{1-y}Co_y]O_2$ solid solution samples.

and the average oxidation state of the transition metal ions are given in Table 1. For example, while the nominal composition for the $y = 0.5$ and $z = 0.7$ sample is $Li[Li_{0.1}Mn_{0.2}Co_{0.35}Ni_{0.35}]O_2$, the observed composition is $Li[Li_{0.05}Mn_{0.21}Ni_{0.37}Co_{0.37}]O_2$ with a loss of a small amount of lithium while maintaining the ratio among the transition metal ions as in the nominal composition.

Figure 10 compares the first charge−discharge profiles of the $(1 - z)Li[Li_{1/3}Mn_{2/3}]O_2 \cdot (z)Li[Ni_{1-y}Co_y]O_2$ ($0.2 \leq z \leq 0.7$) solid solution samples with $y = 0.5$. While the Ni to Co ratio is kept at 1:1, the proportion of $LiNi_{0.5}Co_{0.5}O_2$ to $Li[Li_{1/3}Mn_{2/3}]O_2$ (z value) is varied in this series. The first charge and discharge capacity values of this series of samples are given in Table 1. Figure 11a shows the variations of the first charge capacity in regions A and B and the calculated oxygen loss with lithium content η in the transition metal layer for the $y = 0.5$ series of samples. The initial sloping region A increases with increasing z in Table 1 (or decreasing lithium content η in the transition metal layer in Figure 11a) as a result of an increase in $Ni^{2+/3+}$ and Co^{3+} contents (or a decrease in the average oxidation state of transition metal ions) and their oxidation during first charge, while the plateau region B decreases with increasing z in Table 1 (or decreasing lithium content η in the transition metal layer in Figure 11a) except for the $z = 0.2$ sample due to a decrease in the amount of oxygen loss similar to that found in the previous series of $(1 - z)Li[Li_{1/3}Mn_{2/3}]O_2 \cdot (z)Li[Mn_{0.5-y}Ni_{0.5-y}Co_{2y}]O_2$ samples. A smaller plateau region B and lower total charge and discharge capacities than those expected on the basis of the calculated amount of oxygen loss at low z contents are due to an increasing amount of electrochemically inactive Mn^{4+} and the consequent decrease in the oxygen mobility to leave the lattice similar to that found in the previous series of samples. An interplay between the relative changes in the regions A and B makes the variations in the discharge capacity with z less significant than that in the previous series of samples.

Figure 11b shows the variations of the first charge capacity in regions A and B and the calculated oxygen loss with lithium content η in the transition metal layer of $(1 - z)Li[Li_{1/3}Mn_{2/3}]O_2 \cdot (z)Li[Ni_{1-y}Co_y]O_2$ ($0 \leq y \leq 1$) solid solution samples for $z = 0.5$, and the first charge and discharge capacity values are given in Table 1. While the $Li[Li_{1/3}Mn_{2/3}]O_2$ to $Li[Ni_{1-y}Co_y]O_2$ ratio is kept constant at 1:1, the Co content y in $Li[Ni_{1-y}Co_y]O_2$ is varied from 0 to 1 in this series. The initial sloping region A decreases with increasing Co content y as a result of an increase in the average oxidation state of the transition metal ions, resulting from a decrease in the volatilization of lithium during synthesis. On the other hand, the plateau region B increases with Co content y as a result of an increase in the lithium content in the transition metal layer and the amount of oxygen that could be lost from the lattice. The increase in the amount of oxygen lost (or the plateau region B) leads to an increase in the first total charge capacity and discharge capacity with increasing Co content y.

The data with the two series of samples presented in this section also demonstrate that the amount of oxygen loss from the lattice is determined by the amount of lithium in the transition metal layer. Also, a good agreement between the observed and calculated charge capacities in the sloping region A in these two series of samples as well confirm that the oxygen evolution from the lattice begins for oxidations beyond approximately $Co^{3.6+}$. Additionally, the $(1 - z)Li[Li_{1/3}Mn_{2/3}]O_2 \cdot (z)Li[Ni_{1-y}Co_y]O_2$ samples with $z \approx 0.5$ and $y \approx 0.5$ are found to exhibit a maximum in the irreversible capacity loss values. With a constant value of $z = 0.5$, either an increase in y above 0.5 (increase in Co content) or a decrease in y below 0.5 (increase in Ni content) decreases the irreversible capacity loss.

Conclusions

The irreversible oxygen loss during the first charge from the layered solid solutions between Li[Li$_{1/3}$Mn$_{2/3}$]O$_2$ and Li[M]O$_2$ (M = Mn, Co, and Ni) have been found to be determined by the amount of lithium in the transition metal layer before charge by investigating systematically five different series of samples in the $(1 - z)$Li[Li$_{1/3}$Mn$_{2/3}$]O$_2$·(z)Li[Mn$_{0.5-y}$Ni$_{0.5-y}$Co$_{2y}$]O$_2$ and $(1 - z)$Li[Li$_{1/3}$Mn$_{2/3}$]O$_2$·(z)Li[Ni$_{1-y}$Co$_y$]O$_2$ systems. The lithium content in the transition metal layer is, however, sensitively influenced by the tendency of Ni^{3+} to get reduced to Ni^{2+} and the consequent volatilization of lithium during synthesis. The amount of oxygen loss during first charge in turn influences the reversible capacity values in subsequent cycles. Furthermore, while Ni^{2+} could be fully oxidized to Ni^{4+}, the oxygen loss begins to occur for oxidations beyond $Co^{3.6+}$ as a result of a significant overlap of the $Co^{3+/4+}$:3d band with the top of the O^{2-}:2p band. Although no clear, unified trend could be established for the irreversible capacity loss, it was found to have a maximum value around $z = 0.5$ and $y = 0.5$ in the $(1 - z)$Li[Li$_{1/3}$Mn$_{2/3}$]O$_2$·(z)Li[Ni$_{1-y}$Co$_y$]O$_2$ system. The study shows that the electrochemical performance factors of the Li[Li, Ni, Mn, Co]O$_2$ cathodes could be maximized by optimizing the contents of the various ions.

Acknowledgment. Financial support by NASA and the Welch Foundation Grant F-1254 is gratefully acknowledged.

CM070389Q